

Monoclinic $\text{Li}_{1+x}\text{V}_3\text{O}_8$ Synthesized via Electrospinning and Used as Cathode Material for Lithium Ion Batteries

Feng Wu, Ying Lu, Ying Bai*, Chengshuai Lu, Chuan Wu

Beijing Key Laboratory of Environment Science and Engineering, School of Material Science and Engineering, Beijing Institute of Technology, Beijing 100081, China

*email: membrane@bit.edu.cn

Keywords: Lithium Ion Battery; $\text{Li}_{1+x}\text{V}_3\text{O}_8$; Electrospinning; Electrochemical Performance

Abstract. Monoclinic $\text{Li}_{1+x}\text{V}_3\text{O}_8$ is an attractive cathode candidate for lithium-ion batteries. Here $\text{Li}_{1+x}\text{V}_3\text{O}_8$ precursor was synthesized via a electrospinning process using LiNO_3 , NH_4VO_3 and citric acid as raw materials, and followed by a thermal treatment at 450°C for 5 h in air atmosphere, to get well formed $\text{Li}_{1+x}\text{V}_3\text{O}_8$ powder. The structure, morphology and electrochemical performance of the as-synthesized $\text{Li}_{1+x}\text{V}_3\text{O}_8$ sample were characterized by X-ray diffraction (XRD), fourier transform infrared (FT-IR), scanning electron microscopy (SEM) and galvanostatic charge-discharge test. The effects of synthesis conditions on the structure and the electrochemical performance of the $\text{Li}_{1+x}\text{V}_3\text{O}_8$ sample were evaluated and discussed. It showed a high initial capacity of $283.4 \text{ mAh}\cdot\text{g}^{-1}$, and remained about $210 \text{ mAh}\cdot\text{g}^{-1}$ after 100 cycles.

Introduction

With the development of society and advancements in technology, the lithium ion batteries play an important role in every aspect. Rechargeable lithium ion batteries are considered as one of the simple and effective electrochemical energy storages and transfer systems. They are widely used in portable devices and hybrid electric vehicles [1]. Lithium vanadium oxide (LiV_3O_8) is a promising cathode material for rechargeable lithium batteries. LiV_3O_8 has been constantly researched for its better electrochemical properties in rechargeable lithium batteries because of its high specific energy density, high working voltage and long cycle life [2]. Moreover, the vanadium oxides generally show good chemical stability and better safety characteristics. LiV_3O_8 cathode materials have been synthesized via a hydrothermal improved sol-gel process using LiOH , NH_4VO_3 and oxalic acid as raw materials [2], or oxalic, tartaric, citric and malic acid as the chelating agents [3]. Different types of LiV_3O_8 have been synthesized. Nanorods of LiV_3O_8 have been synthesized using citrate assisted sol-gel method followed by room temperature quenching technique [4]. Rod-like LiV_3O_8 composites have been fabricated by using a carbamide-assisted rheological phase reaction method [1]. Hierarchical plate-arrayed LiV_3O_8 composites have been synthesized by freeze drying method with polyacrylamide (PAM) as surfactant followed by calcination at 500°C [5]. Cookies-shaped LiV_3O_8 materials have been synthesized by a facile ethylene glycol-assisted sol-gel method [6]. Layered LiV_3O_8 as promising cathode material for rechargeable lithium-ion batteries has been synthesized by an improved spray-drying method followed by heating at different temperatures [7] which is dozens of times faster than the conventional route [8]. Ultralong LiV_3O_8 nanowire cathode materials have been synthesized by topotactic Li intercalation are capable of excellent high-rate performance with minimal capacity loss [9]. LiV_3O_8 materials have been prepared with porous state by two different methods, and both the compounds showed excellent electrochemical performance due to their own especial characteristics [10-11]. Recently, a low-temperature thermal co-decomposition method has been used for fabricating a LiV_3O_8 nanorod [12].

Vanadium-based oxides have become one of the most attractive electrode candidates for lithium ion batteries. Among which, $\text{Li}_{1+x}\text{V}_3\text{O}_8$ is the most promising material with high capacity, excellent lithium intercalation performance, long cycling life and lower cost [13-15]. $\text{Li}_{1+x}\text{V}_3\text{O}_8$ can be synthesized by tartaric acid assisted sol-gel method [16], citric acid/tartaric acid assisted sol-gel

method [17], or hydrothermal reaction [18].

In this paper, $\text{Li}_{1+x}\text{V}_3\text{O}_8$ precursor was firstly synthesized via a electrospinning process, then followed by a thermal treatment at 450°C for 5 h in air atmosphere, to get well formed $\text{Li}_{1+x}\text{V}_3\text{O}_8$ powder. The effects of synthesis conditions on the structure and the electrochemical performance of the $\text{Li}_{1+x}\text{V}_3\text{O}_8$ sample were evaluated and discussed

Experimental

Synthesis of $\text{Li}_{1+x}\text{V}_3\text{O}_8$ cathode material

LiNO_3 , NH_4VO_3 and citric acid were dissolved in ethanol and deionized water (the ratio is 1:1) and reacted at 70°C to prepare concentration, then 1.6 g polyvinylpyrrolidone (PVP) were added in to get the solution for electrospinning. The precursor was kept in an oven at 450°C for 5 h in air atmosphere to get cathode materials $\text{Li}_{1+x}\text{V}_3\text{O}_8$. We characterized the product with FTIR, SEM, XRD, and charge/discharge test.

Structural characterization

The crystallographic phase analysis was carried out by UltimaIV-185 X-ray diffractometer with a $\text{Cu/K}\alpha$ radiation at 40 kV and 100 mA with in the diffraction angle (2θ) ranging from 10° to 70° with a scan rate of $8^\circ/\text{min}$. The microstructure and morphology of sample were determined by scanning electron microscope (FEI-SEM, QUANTA 6000).

Electrochemical characterization

Electrochemical performances of $\text{Li}_{1+x}\text{V}_3\text{O}_8$ were carried out by using CR2025 coin-type cells. A metallic lithium foil served as the anode. The cathode consisted of 80 wt.% active material, 10 wt.% acetylene black and 10 wt.% polyvinylidene fluoride (PVDF) on aluminum foil. 1 M LiPF_6 in diethyl carbonate (DEC) -dimethyl carbonate (DMC) -ethyl methyl carbonate (EMC) (1:1:1 in volume) was used as the electrolyte, and a polypropylene micro-porous film (Cellgard 2300) was used as the separator. The cells were assembled in an argon-filled glove box with H_2O and O_2 concentrations less than 0.5 ppm. The charge-discharge tests were conducted between 2.0 and 4.2 V at room temperature, on LAND battery tester (Wuhan, China).

Results and discussions

FTIR analysis of the precursor and the as-synthesized $\text{Li}_{1+x}\text{V}_3\text{O}_8$

Fig.1 show the FTIR spectra of the precursor and the as-synthesized $\text{Li}_{1+x}\text{V}_3\text{O}_8$ sample, respectively. In Fig.1 (a) the stretching vibration of N-H in the ammonium appears at 3480 cm^{-1} , while the stretching vibration of O-H in the carboxylate appears at 3200 cm^{-1} . Peak 1640 cm^{-1} and 1385 cm^{-1} are caused by the stretching vibration of COO^- in the carboxylate, and the absorption peak at 1640 cm^{-1} also includes the stretching vibration of C=O in amide bond. The absorption peak at 995 cm^{-1} was the stretching vibration of V=O . The absorption peak at 865 cm^{-1} was a typical reflection of V=O in the short-range order, while 655 cm^{-1} was a typical reflection of V-O-V in the long-range order [19].

In Fig.2 (b) the main absorption peak is located in the fingerprint region. The three absorption peak located between 1000 cm^{-1} and 956 cm^{-1} are assigned by the three V=O bond stretching vibration in the $\text{Li}_{1+x}\text{V}_3\text{O}_8$ crystal cell [20]. The absorption peak at 755 cm^{-1} is caused by the vibration of the oxygen atom $\text{O}(3)$ which is between the VO_6 octahedral and VO_5 trigonal bipyramid [21]. The absorption peak at 590 cm^{-1} is caused by the bending vibration of V=O and V-O-V [22].

The FTIR spectra indicate that after calcination, the complexes and PVP in the sample precursor are decomposed, and $\text{Li}_{1+x}\text{V}_3\text{O}_8$ crystal is well formed.

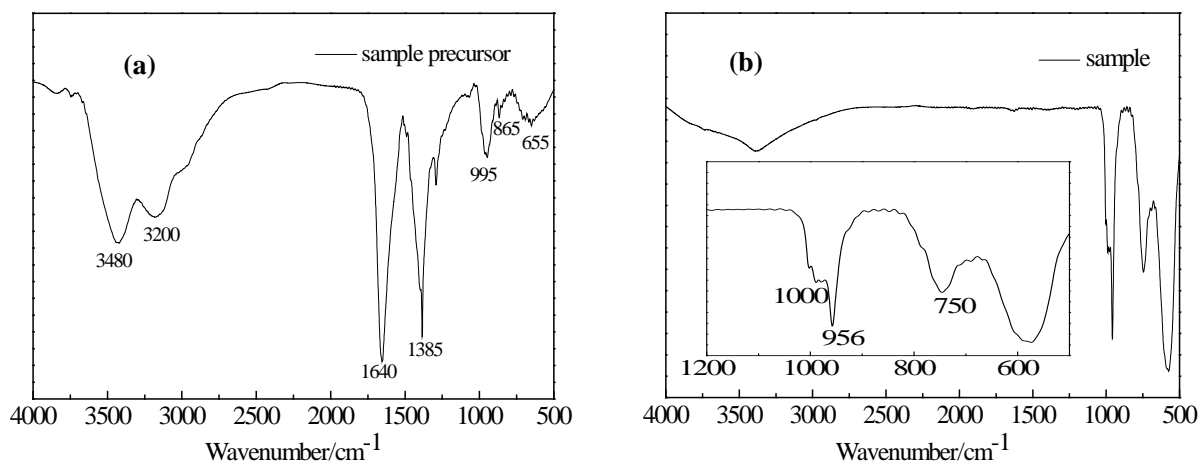


Fig.1. FTIR spectra of (a) the precursor prepared by the electrospinning process, and (b) the as-synthesized $\text{Li}_{1+x}\text{V}_3\text{O}_8$.

Apparent morphology analysis

Fig.2 shows the SEM images of the precursor and the as-synthesized $\text{Li}_{1+x}\text{V}_3\text{O}_8$ sample. As shown in Fig.2 (a), the sample precursor is composed by fibrous xerogel, whose diameter is main in the range of 1 to 1.5 μm . Differences in diameter may be caused by the inconsistency of the jet solvent evaporation rate in the electrostatic field. The length of the sample precursor observed under the low magnification is up to several hundred microns, while the sample is the rod-shaped material under the scanning electron microscope. After being calcined at 450°C, the as-synthesized $\text{Li}_{1+x}\text{V}_3\text{O}_8$ shows different apparent morphology, with many solid rods and blocks in the size from 0.5 to 1 μm , as shown in Fig. 2(b). The gaps between the constituent units make the stick internal have more space, which can do good to the contact of $\text{Li}_{1+x}\text{V}_3\text{O}_8$ particles with the electrolyte.

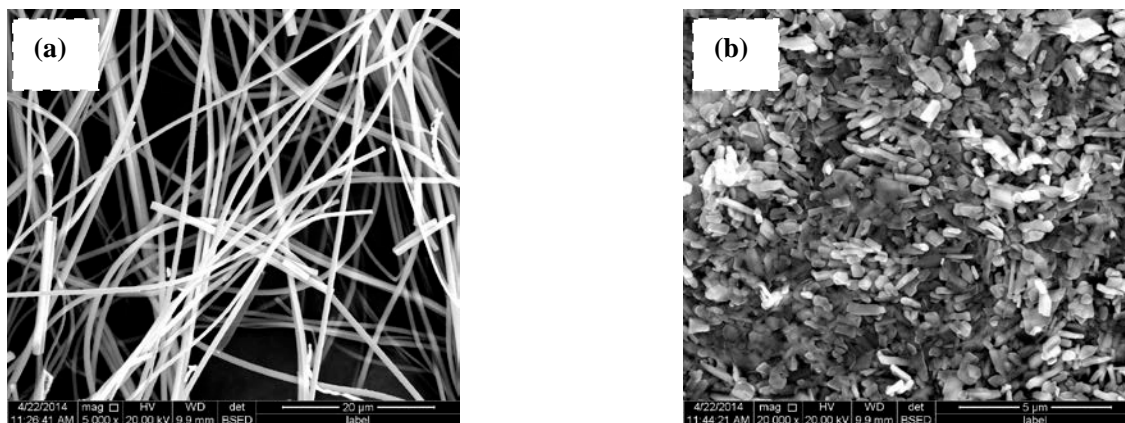


Fig.2. SEM images of (a) the precursor prepared by the electrospinning process, and (b) the as-synthesized $\text{Li}_{1+x}\text{V}_3\text{O}_8$.

Crystal structural analysis

The XRD pattern of the $\text{Li}_{1+x}\text{V}_3\text{O}_8$ sample is shown in Fig.3. Comparing with LiV_3O_8 standard PDF card (JCPDS:72-1193), it is found that the high degree of agreement between the two patterns, and no obvious miscellaneous peaks which indicate that there are very few impurities in the sample. The main diffraction peaks in XRD pattern of the sample correspond to the main plane of LiV_3O_8 , in which the greatest impact on the electrochemical performance is (100) diffraction. Here the (100) diffraction n peak is very strong, indicating that the as-synthesized $\text{Li}_{1+x}\text{V}_3\text{O}_8$ sample has a well-developed crystalline structure, which is closely related to the embedded rate of lithium ions. The (100) diffraction peak of the sample has the maximum relative strength, which indicates that a relatively longer diffusion path for lithium ions embedded and extrusion can be provided between (100) and other diffractions, while for a layered structure of $\text{Li}_{1+x}\text{V}_3\text{O}_8$, the lithium ions embedded is a diffusion process, therefore, a longer diffusion path is negative for lithium ion embedded and

extrusion .The (100) diffraction peak here is at $2\theta = 13.913^\circ$, which is in keeping with the standard card angle diffraction peak ($2\theta = 13.915^\circ$).

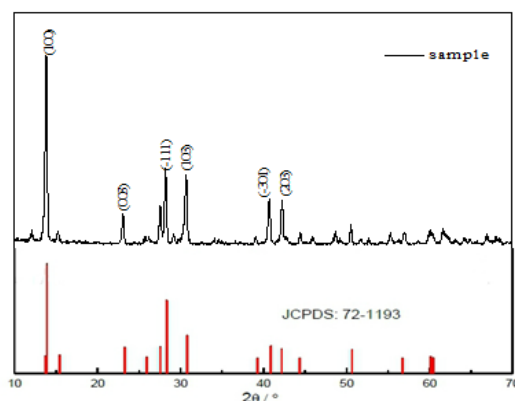


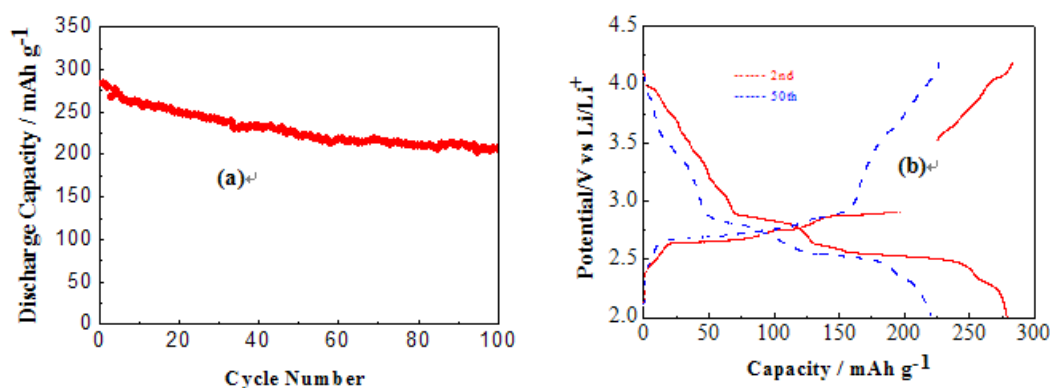
Fig.3. XRD pattern of the as-synthesized $\text{Li}_{1+x}\text{V}_3\text{O}_8$ sample.

Electrochemical performances

Fig.4. Electrochemical performances of the $\text{Li}_{1+x}\text{V}_3\text{O}_8$ sample. (a) The cycling performance at 0.1C. (b)The second and 50th charge-discharge curves. (c) Rate performances at various current densities.

Fig.4 (a) shows the charge-discharge capacity of the sample in 0.1 C ($28 \text{ mAh}\cdot\text{g}^{-1}$) current density and the range of 2.0 to 4.2 V. The sample has a high initial discharge capacity of $283.4 \text{ mAh}\cdot\text{g}^{-1}$. The capacity decreases slowly with the constantly charging and discharging, which is due that the process of lithium ions embedding and prolapse damages the part of the crystal structure, while irreversible phase transition from LiV_3O_8 to $\text{Li}_4\text{V}_3\text{O}_8$ reduces the number of prolapsed lithium ion. After the 100 cycle the discharge capacity is about $210 \text{ mAh}\cdot\text{g}^{-1}$. It indicates that the sample has a high discharge capacity and good cycle performance.

Fig.4 (b) shows the second cycle and 50th cycle charge and discharge curve of the sample. The charge-discharge curve has several charging and discharging platforms, the main discharge platforms are near 2.8 V and 2.6 V. The second charge curve has 2.3 V, 2.6 V, 3.1 V, 3.35 V and 4.0 V five platforms, but in the 50th charge curve only the platform at 2.6 V has no change. The second discharge curve has 4.0 V, 3.6 V, 2.8 V, 2.6 V four platforms, but in the 50th discharge curve 2.8 V platform decreases to 2.6 V and 2.6 V platform decreases to 2.5 V. For the 50th cycle, when being compared with the second cycle, the decrease of the discharge capacity is due to the capacity fading of 2.8 and 2.6 V platforms, which may be related to an irreversible phase transition of the $\text{Li}_{1+x}\text{V}_3\text{O}_8$.



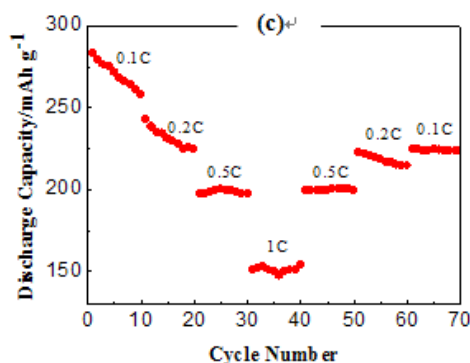


Fig.4 Electrochemical performances of the $\text{Li}_{1+x}\text{V}_3\text{O}_8$ sample.

The rate performances of the $\text{Li}_{1+x}\text{V}_3\text{O}_8$ are evaluated at various current densities from 0.1 to 1 C, and then gradually back to 0.1C, as shown in Fig.4(c). At 0.1 C rate, the discharge capacity falls from $283.4 \text{ mAh}\cdot\text{g}^{-1}$ to $258 \text{ mAh}\cdot\text{g}^{-1}$ in the first 10 cycle, and the discharge capacity remains stable in the last 10 cycle which is close to $250 \text{ mAh}\cdot\text{g}^{-1}$. At 0.2 C, the discharge capacity is near $220 \text{ mAh}\cdot\text{g}^{-1}$, while at 0.5 C the discharge capacity is near $200 \text{ mAh}\cdot\text{g}^{-1}$. At 1 C the discharge capacity is around $150 \text{ mAh}\cdot\text{g}^{-1}$.

Conclusions

$\text{Li}_{1+x}\text{V}_3\text{O}_8$ precursor is prepared by an electrospinning process, where mixed ethanol and deionized water (the ratio is 1:1) is used as a co-solvent of the spinning solution. The precursor is composed with 1 to $1.5 \mu\text{m}$ wide and a few hundred micrometers long fibers, which can get uniform small $\text{Li}_{1+x}\text{V}_3\text{O}_8$ particles after calcination at 450°C . The as-synthesized $\text{Li}_{1+x}\text{V}_3\text{O}_8$ sample shows rod-like morphology, which is composed with small size rods or blocks. XRD analysis shows that it has a pure monoclinic phase. The $\text{Li}_{1+x}\text{V}_3\text{O}_8$ achieves a high initial discharge capacity of $283.4 \text{ mAh}\cdot\text{g}^{-1}$ at 0.1 C, as well as a good cycling performance. It indicates that the $\text{Li}_{1+x}\text{V}_3\text{O}_8$ prepared by electrospinning can efficiently control the morphology, result in good electrochemical performance, and therefore is a promising cathode material for lithium ion batteries.

Acknowledgements

The present work was supported by the National 973 project (No. 2015CB251100), the Program for New Century Excellent Talents in University (Grant NCET-12-0047), and Beijing Higher Institution Engineering Research Center of Power Battery and Chemical Energy Materials.

References

- [1] Qiao, Y. Q.; Wang, X. L.; Zhou, J. P.; Zhang, J.; Gu, C. D.; Tu, J. P., *J. Power Sources* 198 (2012) 287-293.
- [2] Wang, D. Q.; Cao, L. Y.; Huang, J. F.; Wu, J. P., *Ceram. Int.* 38 (4) (2012) 2647-2652.
- [3] Wang, D. Q.; Cao, L. Y.; Huang, J. F.; Wu, J. P., *Ceram. Int.* 39 (2013) 3759-3764.
- [4] Sarkar, S.; Banda, H.; Mitra, S., *Electrochim. Acta* 99 (2013) 242-252.
- [5] Huang, S.; Lu, Y.; Wang, T. Q.; Gu, C. D.; Wang, X. L.; Tu, J. P., *J. Power Sources* 235 (2013) 256-264.
- [6] Huang, S.; Wang, X. L.; Lu, Y.; Jian, X. M.; Zhao, X. Y.; Tang, H.; Cai, J. B.; Gu, C. D.; Tu, J. P., *J. Alloys Compd.* 584 (2014) 41-46.
- [7] Xiong, X. H.; Wang, Z. X.; Guo, H. J.; Li, X. H.; Wu, F. X.; Yue, P., *Electrochim. Acta* 71 (2012) 206-212.

- [8] Xiong, X. H.; Wang, Z. X.; Li, X. H.; Guo, H. J., *Mater. Lett.* 76 (2012) 8-10.
- [9] Xu, X.; Luo, Y. Z.; Mai, L. Q.; Zhao, Y. L.; An, Q. Y.; Xu, L.; Hu, F.; Zhang, L.; Zhang, Q. J., *NPG Asia Aterials* 4 (2012) 1-7.
- [10] Liu, H. M.; Wang, Y.G.;Yang, W.S.; Zhou, H. S., *J. Electrochim. Acta* 56 (2011) 1392.
- [11] Ma, H.; Yuan, Z. Q.; Cheng, F. Y.; Liang, J.; Tao, Z. L.; Chen, J., *J. Alloys Compd.* 509 (2011) 6030.
- [12] Pan, A.Q.; Liu, J.; Zhang, J. G.; Cao, G. Z.; Xu, W.; Nie, Z. M.;Jie, X.; Choi, D.; Arey, B.W.; Wang, C. M.; Liang, S. Q., *J. Mater. Chem.* 21 (2011) 1153.
- [13] Pistoia, G. M. L.; Di Vona, P.; Tagliatesta., *Solid State Ionics* 24 (1987) 103-109.
- [14] Wu, F.; Wang, L; Wu, C.; Bai, Y.; Wang, F., *Mater. Chem. Phys.* 115 (2-3) (2009) 707-711.
- [15] Liu, H. M.; Wang, Y. G.; Wang, K. X.; Wang, Y. R.; Zhou, H. S., *J. Power Sources* 192 (2) (2009) 668-673.
- [16] Shui, M.; Zheng, W. D.; Shu, J.; Wang, Q. C.; Gao, S.; Xu, D.; Chen, L. L.; Feng, L.; Ren, Y. L., *Mater. Res. Bull.* 47 (2012) 2455–2459.
- [17] Shui, M.; Zheng, W. D.; Shu, J. ; Wang, Q. C.; Gao, S.; Xu, D.; Chen, L. L.; Feng, L.; Ren, Y. L., *Curr. Appl. Phys.* 13 (2013) 517-521.
- [18] Kyungho, K.; Su, H. P.; Tae, H. K.; Hyungkeun, A.; Yang D. E.; Lee, M. J., *Ceram. Int.* 39 (2013) 1623-1629.
- [19] Kawakita, J.; Katayama Y.; Miura T.; Kishi, T., *Solid State Ionics* 110 (1998) 199-207.
- [20] Yang, G.; Wang, G.; Hou, W., *Phys. Chem. B* 109 (2005) 11186-11196.
- [21] Zhang, X.; Frech. R.. J., *Electrochim. Acta* 43 (1998) 861-868.
- [22] Tossici, R.; Marassi, R.; Berrettoni, M.; Stizza, S.; Pistoia, G., *Solid State Ionics* 57 (1992) 227-234.